Renewable Energy 138 (2019) 876–890

Contents lists available at ScienceDirect

Renewable Energy

journal homepage: www.elsevier.com/locate/renene

Performance enhancement of the photovoltaic cells using Al_2O_3/PCM mixture and/or water cooling-techniques

M.R. Salem*, M.M. Elsayed, A.A. Abd-Elaziz, K.M. Elshazly

Benha University, Faculty of Engineering at Shoubra, Mechanical Engineering Department, 108 Shoubra Street, Cairo 11689, Egypt

ARTICLE INFO

Article history:
Received 13 December 2018
Received in revised form
25 January 2019
Accepted 7 February 2019
Available online 10 February 2019

Keywords:
Photovoltaic
Electrical
Thermal and exergy efficiencies
Nanoparticles
PCM

ABSTRACT

This work experimentally investigates the performance of a PV module cooling effect using a compound enhancement technique. This is by employing water and/or Al_2O_3/PCM mixture with different nanoparticles mass concentrations (φ) from 0 to 1% and mass fluxes of the cooling water from 0 to 5.31 kg/s.m^2 through straight aluminium channels beneath the PV panel. The effect of the occupation ratio of the Al_2O_3/PCM (λ_{PCM}) in the channels from 0 (100% water) to 100% (0% water) is also examined. The results illustrate that the Al_2O_3 nanoparticles of $\varphi = 1\%$ makes the compound technique (Al_2O_3/PCM mixture + water) better than the cooling with 100% water. Compared with all studied cooling techniques parameters, it is observed that the compound technique; Al_2O_3($\varphi = 1\%$)/PCM mixture ($\lambda_{PCM} = 25\%$) + 75% water (5.31 kg/s.m^2) achieves the highest PV performance. However, although the Al_2O_3/PCM mixture of $\lambda_{PCM} = 100\%$ does not provide the highest PV electrical output power, it may be a superior solution for the PV cooling as it solves the problems of using the cooling water. Finally, experimental correlations are presented to predict the electrical, thermal, and overall exergy efficiencies of the PV cell.

1. Introduction

Improving the performance of electrical power production systems is an important challenge facing many economies. PV modules are one of the most promising power generation systems, nevertheless, the high cost of PV power generation besides its lower efficiency restrict the progress of the PV cells industry. The PV conversion efficiency of light into electrical power depends on numerous constraints including its temperature; the output power decreases by 0.2–0.5% per 1 K increase in the PV panel temperature [1]. Therefore, most researchers concentrated their interest in augmenting the PV modules cooling to boost the electrical efficiency. Two main methods were introduced to do the desired heat transfer rate; *passive* and *active* techniques. Moreover, any at least two of these techniques (passive and/or active) might be utilized simultaneously to get enhancement in the heat exchange that is more remarkable than that resulted by just a single technique itself. This synchronous use is named *compound* technique [2–4].

In the passive approaches, many studies investigated the effect of integrating a heat pipe to the PV-rear surface [5–7]. Tonui and Tripanagnostopoulos [8] numerically simulated the cooling of a module by a natural air flow besides conducting fins. Another field of the PV passive cooling is utilizing PCMs. Huang et al. [9–11] used a paraffin wax in a rectangular vessel appended to the back surface of the module, which reduced the PV temperature by more than 3 °C. Huang [12] experimentally and numerically investigated the thermal regulation of a PV-PCM system in triangular shaped cells under static state and realistic conditions. Ho et al. [13] carried out numerical simulations for the performance of a PV module integrated with a microencapsulated PCM layer. The results indicated that the PCM revealed a good cooling response. Hasan et al. [14] experimentally recorded that using the PCM enhanced the electrical efficiency by about 10% and 10.7% in Ireland and Pakistan, respectively. Machniewicz [15] simulated numerically the PV panel cooling using PCM. The results showed an enhancement in the electrical efficiency by 10%. Hachem et al. [16] presented an experimental investigation on the effect of using pure and combined PCM/copper/graphite on the performance of a PV panel. A maximum enhancement in the PV electrical efficiency of 5.8% was achieved using the combined PCM. Tan et al. [17] indicated that the surface temperature was reduced by 15 °C while the electrical efficiency was improved by 5.39% for finned-PCM panels. Hasan et al. [18] indicated an enhancement of 5.9% in the electrical efficiency using PCM-cooling. Nada et al. [19] investigated the effect of

* Corresponding author.
E-mail addresses: me_mohamedreda@yahoo.com, mohamed.abdelhamid@feng.bu.edu.eg (M.R. Salem).

https://doi.org/10.1016/j.renene.2019.02.032
0960-1481/

integrating Al_2O_3/PCM (51–57 °C melting temperature) to the back surface of PV panel. It was shown that the maximum reduction in the cells temperature of 10.6 °C was resulted, which augmented their electrical efficiency by 13.2%. Khanna et al. [20] introduced a mathematical model to examine the performance characteristics of a finned-PV/PCM system. Khanna et al. [21] experimentally found that PV temperature was decreased by 19 °C using PCM and the electrical efficiency was augmented by 11.1%. Yang et al. [22] experimentally tested the performance characteristics of a PVT/PCM system. They authors assured that the addition of the PCM layer to the PVT cell augmented the thermal and power performances.

In addition, numerous researchers devoted their attention to the active cooling approaches using a hybrid photovoltaic/thermal (PVT) solar system to yield both electric and heat energies from one united module. Joshi and Tiwari [23] presented an exergy analysis of a PVT/air collector. The exergy and thermal efficiencies were 12–15% and 55–65%, respectively. Abdolzadeh and Ameri [24] examined the performance attributes due to spraying water over the top surface of the module. They recorded an enhancement in the electrical efficiency by 3.26%. Teo et al. [25] indicated that the electrical efficiency was augmented by 14% with passing air in parallel conduits behind the panel. Elmir et al. [26] numerically indicated that using Al_2O_3/water nanofluid behind the cell enhanced its cooling. Bahaidarah et al. [27] practically demonstrated that the PV electrical efficiency was enhanced by 9% using water at PV-back surface, while Ozgoren et al. [28] found that it was increased from 8% to 13.6%. Ceylan et al. [29] observed an increase in the electrical efficiency from 10% to 13% by conducting a simple copper pipe behind the PV module. Karami and Rahimi [30] estimated the heat transfer attributes in a cell using Boehmite nanofluid in straight and helical channels. Compared with pure water, the uppermost electrical efficiency was enhanced by 37.7% for the helical channel. Aldihani et al. [31] examined the performance of a PV-panel under Kuwait environment. The estimations demonstrated that the dust dropped the output power by 16%. Nizetic et al. [32] observed an augmentation of 16.3% in the electrical efficiency by applying water spray on the PV surface. Salem et al. [33] examined the PV-cooling using water flow through straight/helical channels. The experiments revealed that maximum increments in the electrical and thermal efficiencies of 38.4% and 57.9%, respectively, were achieved using the helical configuration. Preet et al. [34] investigated the effect of applying water-based PVT and water-based PVT/PCM systems. In the later cooling system, the water flows in circular tubes behind the cell. It was demonstrated that the peak temperature decrease was 53% for water-based PVT/PCM.

From this literature survey, it is illustrated that there are numerous cooling techniques that were proposed to enhance the PV performance. One of these techniques is using the PCM, which achieved an acceptable enhancement compared with water active cooling in numerous countries. Therefore, this work is firstly devoted to experimentally compare the PV performance under cooling with water (active technique) or PCM (passive technique), with an uncooled one, in the climatic conditions during summer months in Cairo, which is considered one of the most energy-consuming areas in Egypt where a promising solar intensity is found. Secondly, the proposed research aims to test the effect of water/PCM occupation ratio in channels conducted at the PV-rear surface, in addition to the influence of adding Al_2O_3 nanoparticles to the PCM on the PV performance characteristics. Finally, this work aims to propose experimental relations to predict the module electrical (η_e), thermal (η_{th}) and overall exergy ($\eta_{o,\,ex}$) efficiencies as functions in the investigated parameters.

2. Experimental apparatus

The apparatus (Figs. 1 and 2) used in the present investigation comprises two identical poly-crystalline type 50-Watt PV modules, adjusted stand, the cooling system, and the measuring devices. Table 1 presents the PV module specifications. The cold water (supplied to the channels beneath the cell) circuit consists of a cooling unit, DC pump, valves, water flow meter, and the connecting pipes. To synchronize with the latitude of Cairo where the experiments are conducted, the panels are south adjusted and oriented 30° with the horizontal surface.

Aluminium channels are fabricated and used either for passing the cooling water or are filled with the Al_2O_3/PCM mixture. Twenty individual straight channels of the same length of the cell (670 mm) are constructed with an aspect ratio (depth/width) of 1 with dimensions shown in Fig. 3.

The channels are arranged side by side as illustrated in Fig. 4 and are situated directly under the panel. To reduce the thermal contact resistance, silicon oil is chosen as a thermally conducting liquid, and is applied on the top surface of the channels and on the rear surface of the module before they are pressed against each other. Forty ball valves are employed at the channels inlets and exits to adjust the water flow rate, in addition, to keep the PCM in each channel. The rear surface of the channels is thermally insulated using a 1-inch fibre glass.

An organic solution PCM type (Calcium chloride hexahydrate; $CaCl_2H_{12}O_6$) is utilized in the current investigation with technical specifications illustrated in Table 2. Before charging the channels, the PCM is liquefied through a heating process in a water path until reaching its melting point. Then, the selected channels are fully charged with the liquid PCM. Preparing of a homogeneous mixture of nanoparticles in the PCM liquid is the first step in applying the Al_2O_3/PCM mixture as a heat transfer tool. The particles used in the experiments are gamma-alumina ($\gamma-Al_2O_3$) nanopowders; 99.99%

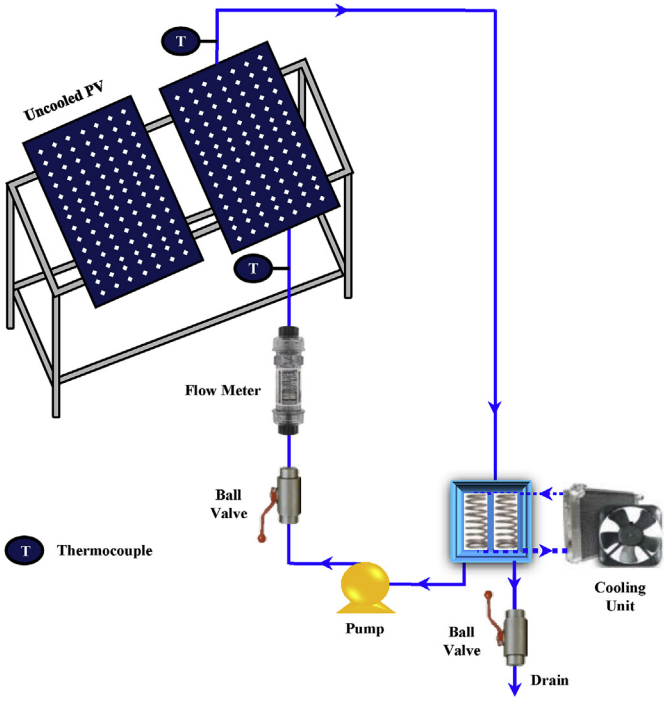

Fig. 1. Schematic representation of the experimental facility.

Fig. 2. A photograph of the experimental setup.

Table 1
PV module specifications.

Cell type	Poly-crystalline
Peak power ($P_{e,\ max}$)	50 W
Dimensions	670*550*35 (±1 mm)
Maximum power voltage (V_{mp})	18 V
Maximum power current (I_{mp})	2.78 A
Open circuit voltage (V_{oc})	21 V
Short circuit current (I_{sc})	3.06 A
Maximum system voltage	1000 V
Ordinary operating PV temperature	45 °C

purity, 40 nm average particle size with a surface area >200 m^2/g. The thermophysical properties of $\gamma-Al_2O_3$ nanoparticles are revealed in Table 3. The dispersion of particles in the PCM liquid is done using an agitator bath with four different mass concentrations.

The cooling unit includes a 20 L stainless steel tank. The heat is removed from the water in the cooling tank by a cooling unit. The operation of the cooler is based on a pre-adjusted digital thermostat. The external surface of the tank is thermally insulated. A DC-pump of maximum power consumption of 4.2 W is connected to the cooling tank outlet to feed the channels with the desired flow rate of the water. Through the experimental runs, the PV-current and voltage, the temperatures of panels' upper and back surfaces, water inlet and outlet temperatures, solar irradiation, ambient air-dry bulb temperature and wind speed are recorded. Eighteen calibrated K-type thermocouples are utilized; sixteen are attached at both surfaces of the two cells, while two thermocouples are employed to estimate the inlet and outlet temperature of the cooling water. All thermocouples are connected to a data logger to record the temperatures. A variable area flow meter, 0.002–2 L/min flow rate range, is used to estimate the water flow rate.

3. Experimental procedures

The first step to record the data from the system is to fill the cooling tank with water from the domestic water supply, then the cooling unit and the pump are turned on. The temperature of the water entering the channels (25 ± 0.5 °C) is adjusted by regulating the temperature in the cooling tank through its thermostat. In each experiment, the water from the cooling tank is directed to the channels beneath the module at different flow rates as revealed in Table 4. The flow rate is controlled using the flow meter and the installed valves. The selected channels that pass the water in each experiment are adjusted through their valves, while the other channels are filled with liquid PCM or Al_2O_3/PCM mixture as shown in Fig. 5. In this figure, λ_{PCM} is the fraction of the channels occupied

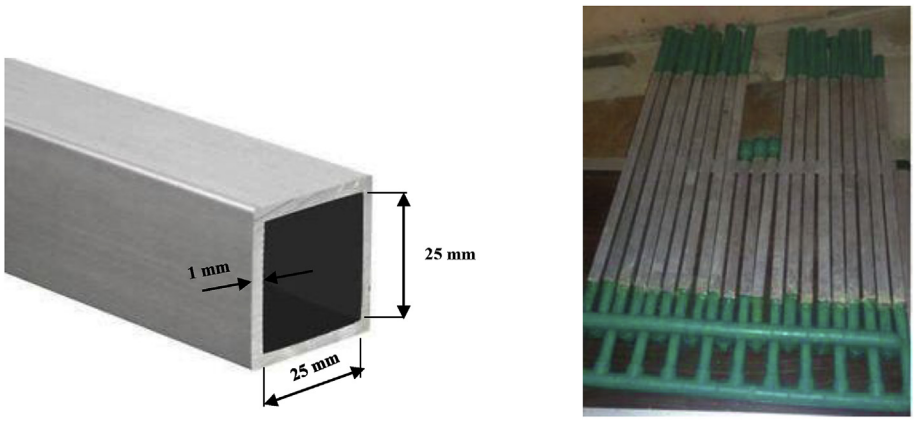

(a) Channel cross section (b) Channels arrangement

Fig. 3. The straight channels.

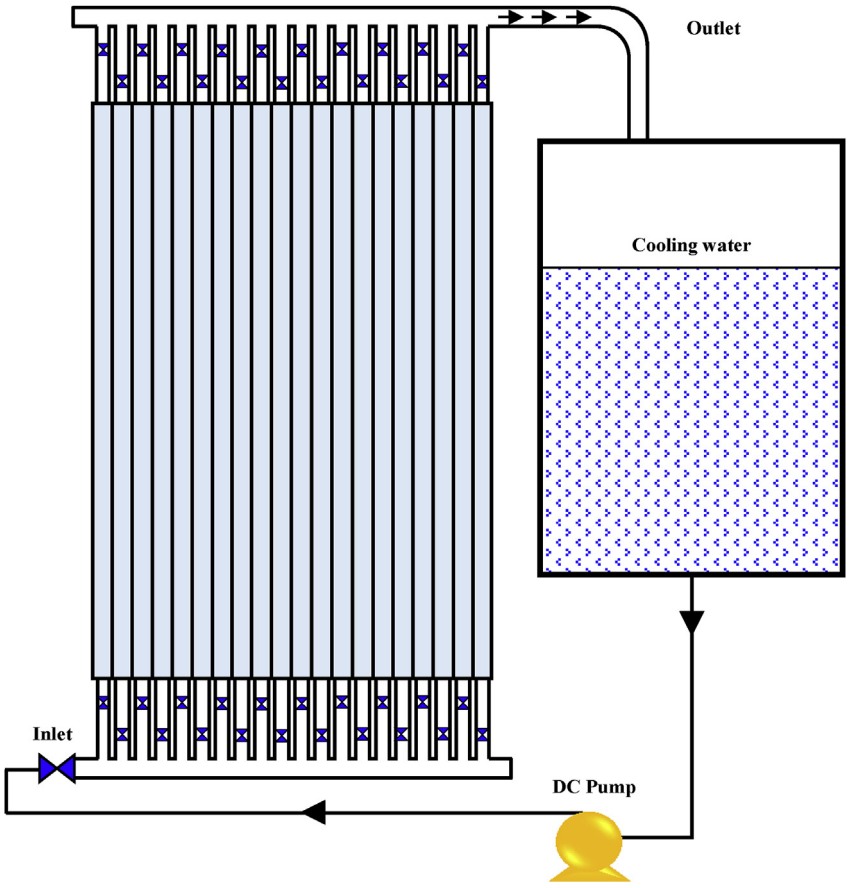

Fig. 4. Schematic representation of the channels cycle.

Table 2
Characteristic specifications of the used PCM.

Type	Calcium chloride hexahydrate; $CaCl_2H_{12}O_6$	
Melting point (°C)	31	
Heat of fusion (kJ/kg)	191	
Thermal conductivity (W/m·°C)	Solid:	1.08
	Liquid:	0.56
Density (kg/m^3)	Solid:	1710
	Liquid:	1560
Specific heat capacity (kJ/kg·°C)	Solid:	1.4
	Liquid:	1.08
Kinematic viscosity (m^2/s)	Liquid:	0.00184
Thermal expansion coefficient (K^{-1})	Liquid:	0.0005

by PCM with respect to the total channels, defined as follow;

$$\lambda_{PCM} = \frac{N_{PCM}}{N_{ch}} = \frac{N_{PCM}}{20} \quad (1)$$

Moreover, the PV surface is cleaned using a dry cloth and the thermocouples are attached to their locations in the system. The two-electric circuit necessary for measuring the two PV characteristics; voltage and current, are assembled as illustrated in Fig. 6. In this figure, the first multimeter (DC-Ammeter) is connected in series with the variable load (Ohm-box), and both are connected in parallel with the second multimeter (DC-Voltmeter). Then, all of them are connected in parallel with the module. After that, the

Table 3
Properties of $\gamma-Al_2O_3$ nanoparticles.

Thermal conductivity (**W**/**m**.°C)	Density (**kg**/**m**^{3})	Specific heat (**J**/**kg**.°C)
36	3600	773

Table 4
Range of operating conditions.

Parameters	Range or value
Cooling water flow rate, L/min	0–1 ($0 \leq M_w \leq 5.31$kg/s.m^2)
Cooling water inlet temperature, °C	25
Ratio of the channels occupied by PCM (λ_{PCM}), %	0–100
Mass concentration of Al_2O_3 nanoparticles in PCM (φ), %	0–1

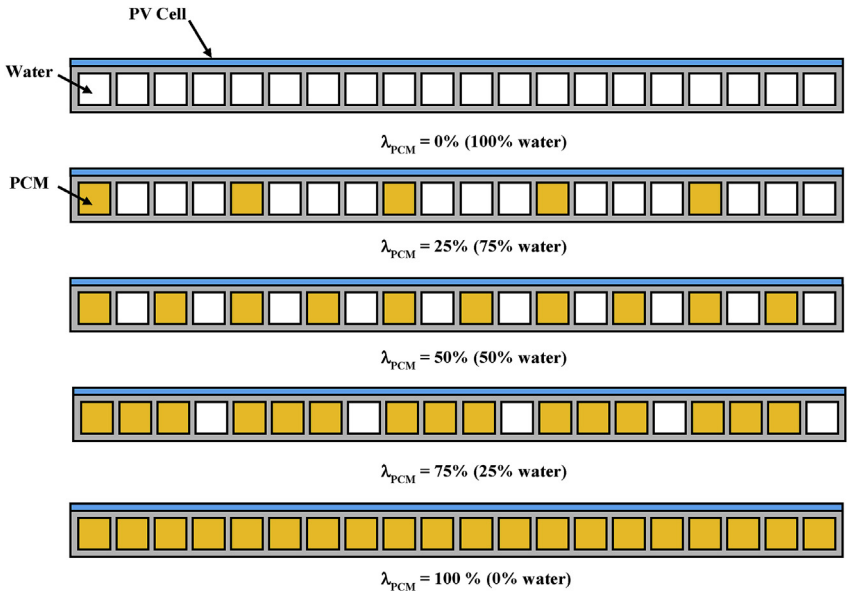

Fig. 5. PCM and water occupation in the channels.

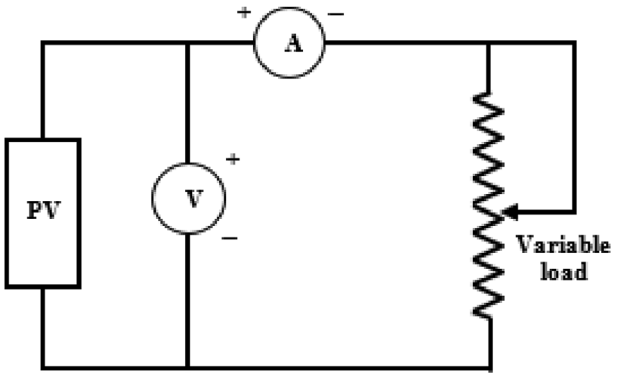

Fig. 6. Measurement circuit for cells characteristics.

variable resistance is set to its greatest value to obtain the *open circuit voltage* (V_{oc}), then the slider is moved gradually to reduce the resistance with recording the variation in the corresponding voltage and current at each point up to reaching the zero-output voltage; *short circuit current* (I_{sc}).

Using the measured PV current and voltage, the I-V characteristic curve is determined, and the electrical power is calculated. Thereby, the maximum power point from the obtained curves is obtained as revealed in Fig. 7. These procedures are started daily at 7 a.m., to let the system to run enough time before collecting the first reading at 8 a.m. At this time, the incident radiation, the modules-surfaces temperatures, cooling water inlet and outlet temperatures, PCM temperature, the ambient dry bulb temperature, and the wind speed are recorded. These measurements are repeated every 30 min till sunset.

4. Al_2O_3/PCM mixture melting point

The temperature at which the Al_2O_3/PCM mixture is melted is measured in the laboratory for different nanoparticles concentrations. A solid piece of the Al_2O_3/PCM mixture is liquefied through a heating process in a water path until reaching its melting point. During the phase change process, the temperature of the mixture is recorded until it is completely liquefied. The melting point is taken as the average of the recorded temperatures. These procedures are repeated three times, from which the mean melting point of the Al_2O_3/PCM mixture is considered. Fig. 8a illustrates the obtained results.

It is evident that the melting point of the pure PCM is 31.2 °C, which is nearly the same as the recorded value by the manufacturer (Table 2). It is clear also that the melting point of the Al_2O_3/PCM mixture is reduced with increasing the nanoparticles concentration to be 25.9 °C at $\varphi = 1\%$. This may be due to increasing the thermal conductivity of the mixture as a result of adding the alumina nanoparticles. Furthermore, the stability of the Al_2O_3/PCM mixture

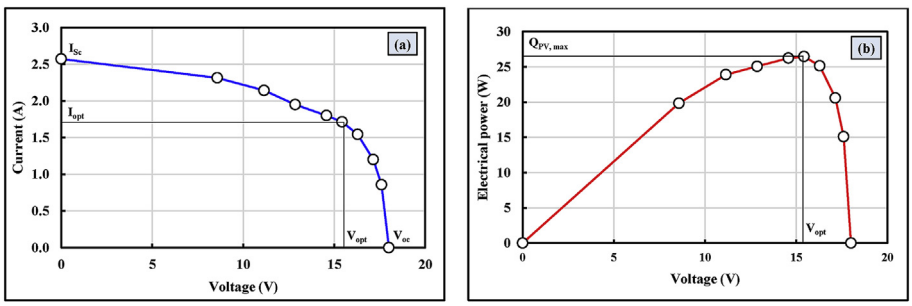

Fig. 7. Characteristic curves for the cell; (a) I-V, (b) P_{PV}-V.

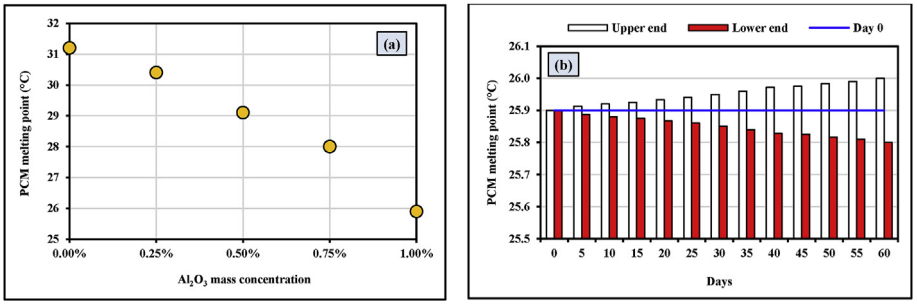

Fig. 8. Average Al_2O_3/PCM mixture melting point; (a) At different nanoparticles concentrations, (b) Over 60 experimental days at $\varphi = 1\%$.

properties is examined to check the effect of multiple melting and re-solidification of the PCM as well as the tilt angle of the cooling system, which may cause a change in the nanoparticles concentration in the PCM from one region to another along the channels. Therefore, the stability of the mixture is verified through the thermal cycling stability testing of the PCM [36,37], by taking a sample of Al_2O_3/PCM mixture from both ends of the tilted channels and measuring its melting temperature within two months with an interval of 5 days. Compared to the melting temperature measured before filling the channels with wax, which preceded the experiments (day 0), tinny deviations in the melting temperature are resulted during this period as shown in Fig. 8b.

5. Data reduction

After knowing the optimum values of the PV-voltage and current, the following relations are utilized to examine its characteristics. The incident solar radiation on the cell is calculated from;

$$P_{in} = G_S \times A_{PV} \tag{2}$$

The maximum module output power is obtained from;

$$P_{PV_{max}} = V_{opt} \times I_{opt} \tag{3}$$

The panel electric efficiency is calculated as follows;

$$\eta_e = \frac{P_{PV_{max}}}{P_{in}} \tag{4}$$

The percentage change in the electrical output power of the cell is calculated as follows [33];

$$\Delta P_e\ (\%) = \left[\frac{P_{PV,\,c} - P_{PV,\,ref} - W_P}{P_{PV,\,ref}}\right] x100 \tag{5}$$

where W_p is the consumed power by the pump, calculated as follows;

$$W_P = V_P \times I_P \tag{6}$$

The rate of the heat energy gained to the water in the channels beneath the PV is obtained from;

$$Q_{th} = \dot{m}_w Cp_w (T_{w,\,o} - T_{w,\,i}) \tag{7}$$

The cooled PV thermal efficiency is calculated as follows;

$$\eta_{th} = \frac{Q_{th}}{P_{in}} \tag{8}$$

The average cell temperature is calculated as follows;

$$T_{PV} = \frac{T_{PV_f} + T_{PV_b}}{2} \tag{9}$$

where T_{PV_f} and T_{PV_b} are the average temperatures of the PV panel top and rear surfaces. Furthermore, Exergy is well-defined as the available energy obtained by subtracting unavailable energy from the total energy. Therefore, the estimation of the exergy efficiency provides a qualitative assessment of the overall performance of the PVT by comparing the electrical and thermal energy based on the same standard [33].

$$\eta_{o,\,ex} = \eta_e + \eta_{th}\left[1 - \frac{T_a}{T_{w,\,o}}\right] \tag{10}$$

T_a is the reference ambient temperature in Kelvin. The mass concentration of the nanoparticles in the PCM is estimated as follows;

$$\varphi = \frac{m_{np}}{m_{total}} = \frac{m_{np}}{m_{np} + m_{PCM}} \tag{11}$$

The cooling water mass flux in each channel (kg/s.m^2) is obtained as follows;

$$M_w = \frac{\dot{m}_W}{A_{ch}} = \frac{\rho_W \dot{V}_W}{(1 - \lambda_{PCM}) N_{ch} * (H_{ch} * W_{ch})} \tag{12}$$

6. Verification of the modules output similarity

Because the cooled and un-cooled panels are tested in parallel, their electrical efficiencies are compared under the same operating conditions for the non-cooling case to test their similarity. The results of the comparison are demonstrated in Fig. 9.

It is seen that there are tiny differences between their electrical efficiencies, which assure that they are identical and can be compared at different cooling conditions.

7. Results and discussions

This work is accomplished through 69 days during which the weather conditions are as follow: average wind speed range is 3.89–4.03 m/s, the average ambient temperature range is 35.4–37.2 °C and average solar radiation intensity range is 632.5–650.8 W/m^2.

7.1. Panel temperature

Fig. 10 illustrates a sample of the recorded panel instantaneous and average temperatures at different occupation ratios of the (Al_2O_3/PCM)/water in the channels from $\lambda_{PCM} = 0\%$ (100% water) to

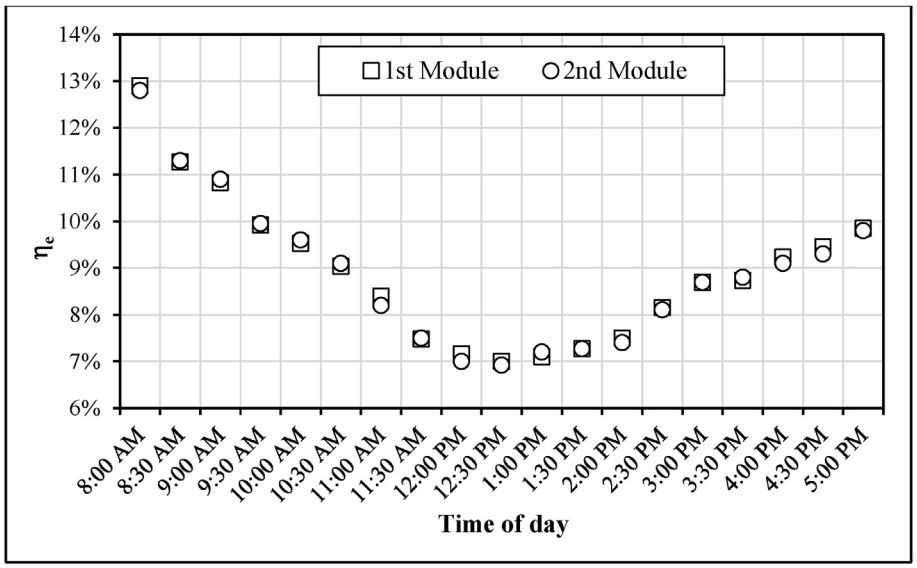

Fig. 9. Comparison between the two panels under the same conditions.

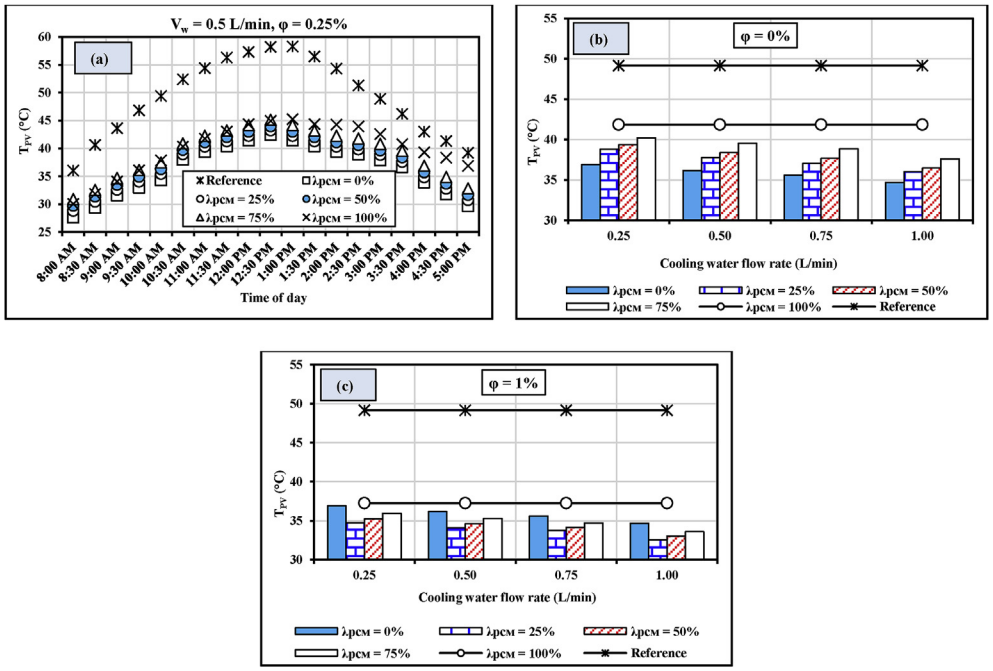

Fig. 10. Panel temperature at different PCM occupation ratios; (a) Instantaneous temperature, (b) Average temperature at φ = 0%, (c) Average temperature at φ = 1%.

$\lambda_{PCM} = 100\%$ (0% water).

From Fig. 10a, it can be seen that the temperature of the panels exhibits the same trend of the solar radiation intensity, which firstly increases until reaching its maximum value at about 1 p.m., and then it drops as the time moves towards the sunset. It is also illustrated that applying the cooling system whether using water and/or Al_2O_3/PCM mixture provides a noticeable drop in cell temperature compared with the uncooled one. In addition, it is noticed that employing $\lambda_{PCM} = 0\%$ results in the lowest module temperature at all times of the day, and its temperature increases gradually with increasing the PCM occupation ratio. Moreover, Fig. 10b and c shows that the average temperature of the modules decreases with increasing the water flow rate; at $\lambda_{PCM} = 0\%$, average drops in the panel temperature of 14.5 °C and 12.3 °C are recorded at $\dot{V}_W = 1.0$ and 0.25 L/min, respectively. This temperature drop is decreased to be 7.4 °C for $\lambda_{PCM} = 100\%$. This is because increasing the water flow rate enhances the rate of heat transfer from the PV and from the PCM to the water, which slows down the phase change process of the PCM, and consequently augments the chance of transferring more heat energy from the cell to the PCM. Fig. 11 illustrates a sample of the recorded cell instantaneous and average temperatures at different nanoparticles mass concentrations in the PCM.

From Fig. 11, it is noticed that the PV temperature decreases gradually with increasing the Al_2O_3 nanoparticles loading in the PCM. This is owing to decreasing the PCM melting point as noticed in Fig. 8, and to increasing the PCM latent heat of fusion with

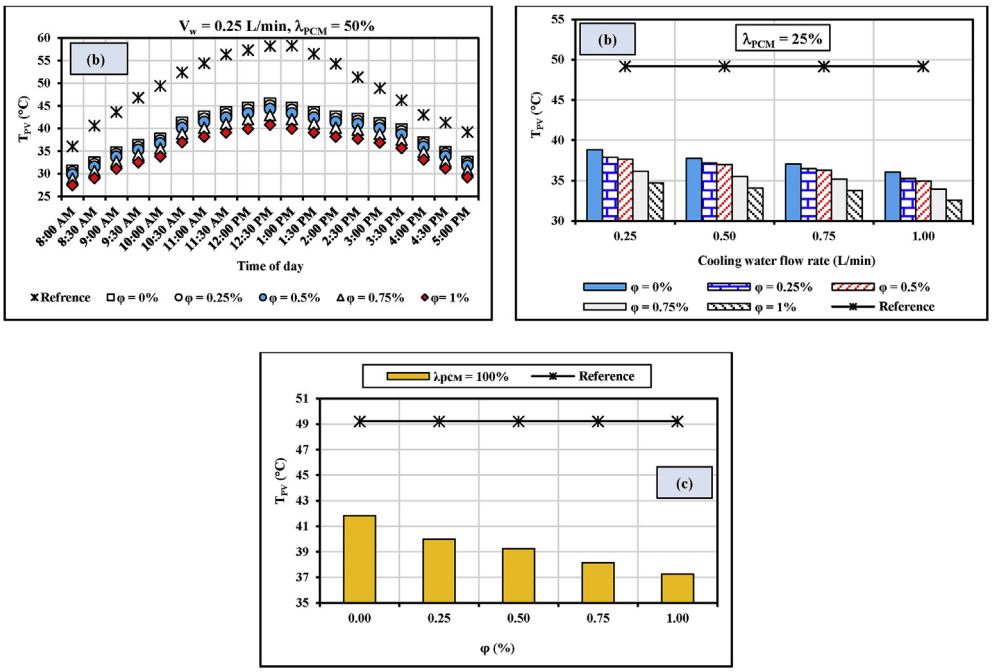

Fig. 11. Panel temperature at different nanoparticles concentrations; (a) Instantaneous temperature, (b) Average temperature at $\lambda_{PCM} = 25\%$, (c) Average temperature at $\lambda_{PCM} = 100\%$.

increasing nanoparticles loading [35]. Furthermore, it is observed that employing $\lambda_{PCM} = 0\%$ provides lower module temperatures at all times of the day when compared with the compound technique; Al_2O_3($\varphi = 0.25\%$ or 0.5%)/PCM mixture + water. It is also shown at $\varphi = 0.75\%$ that the compound technique; $\lambda_{PCM} = 25\%$, provides a cell temperature lower than that at $\lambda_{PCM} = 0\%$ at the same water flow rate. While increasing the nanoparticles concentration to $\varphi = 1\%$, makes the compound technique (Al_2O_3/PCM mixture + water) better than employing 100% water at the conditions. It is clear that $\lambda_{PCM} = 25\%$ ($\varphi = 1\%$) + 75% water (1 L/min) achieves the lowest panel temperature. It is clear also that at $\lambda_{PCM} = 100\%$ ($\varphi = 0.25\%$), an average drop of 9.2 °C in the panel temperature is reported, while this drop increased to be 12 °C at $\varphi = 1\%$. It is evident also that an average drop of 14.5 °C in the panel temperature is recorded at $\lambda_{PCM} = 25\%$ ($\varphi = 1\%$) + 75% water (0.25 L/min) and this increased to be 16.6 °C at $\lambda_{PCM} = 25\%$ ($\varphi = 1\%$) + 75% water (1 L/min).

7.2. Panel electrical efficiency

Fig. 12 demonstrates a sample of the reported instantaneous and average electrical efficiencies of the cooled and uncooled panels at different Al_2O_3/PCM occupation ratios in the channels beneath the module.

It is revealed from Fig. 12 that the cooled cell supplies a higher electrical efficiency than that of the uncooled one. It starts high at 8 a.m. and then decreases to reach its minimum value at nearly 1 p.m. due to the increase in the panel temperature with increasing the incident solar radiation. As the solar radiation intensity is going down later, the electrical efficiency is going up gradually. In addition, it is noticed from Fig. 12a that employing $\lambda_{PCM} = 0\%$ results in the highest electrical efficiency at all times of the day, and this efficiency decreases gradually with increasing the PCM occupation ratio. Furthermore, Fig. 12b and c indicate that the electrical efficiency increases with increasing the water flow rates. At $\lambda_{PCM} = 0\%$, the average electrical efficiency increases from 11.9% to 13% when the water flow rate increases from 0.25 to 1.0 L/min, respectively. Compared with the reference cell ($\eta_e = 8.9\%$), the average percentage increase in the electrical efficiency is 33.4% and 45.5%, respectively. Additionally, when all the channels are 100% employed with pure PCM, the average electrical efficiency is 10.3%, which corresponds to an average percentage increase of 15.7%. Furthermore, Fig. 12 demonstrates that the electrical efficiency decreases gradually with increasing the PCM occupation ratio. Compared with the reference cell, the average percentage increase in the electrical efficiency is 40.5% and 28.8%, at $\lambda_{PCM} = 25\%$ and $\lambda_{PCM} = 75\%$, respectively. In addition, when all the channels are 100% employed with Al_2O_3/PCM mixture, the average electrical efficiency of the panel is 10.9%, which corresponds to a percentage increase of 22.7%.

Fig. 13 shows a sample of the recorded instantaneous and average electrical efficiencies of the panels at different Al_2O_3 nanoparticles concentrations.

It is revealed in Fig. 13 that increasing the nanoparticles concentration in the PCM augments the electrical efficiency of the panels. Compared with the reference cell, the average electrical efficiency increases by 32% and 37.1% at $\varphi = 0.25\%$ and $\varphi = 1\%$, respectively. This due to decreasing the module temperature with increasing the particles concentrations. Compared with $\lambda_{PCM} = 0\%$, the compound technique is better only at $\lambda_{PCM} = 25\%$, with nanoparticles concentrations of 1% and 0.75%, respectively. Fig. 14 presents a comparison for the percentage increase in the module electrical efficiency in the present study, for $\lambda_{PCM} = 100\%$ at $\varphi = 0\%$ and 1%, with that recorded by other researchers at approximate operating conditions. It should be noted that these works used PCM in a cabinet (not channels) behind the panel. It is clearly shown that the present cooling system ($\lambda_{PCM} = 100\%$) gives remarkable enhancement in the electrical efficiency compared with other works. This enhancement can be attributed to the channels walls, which act as fins in addition to the enhanced thermophysical properties of the PCM as a result of adding the nanoparticles.

It is obvious also in Figs. 12 and 13 that the electrical efficiency of the panels, which are cooled with water is higher than that of the cooled panel using $\lambda_{PCM} = 100\%$. While the percentage increase in

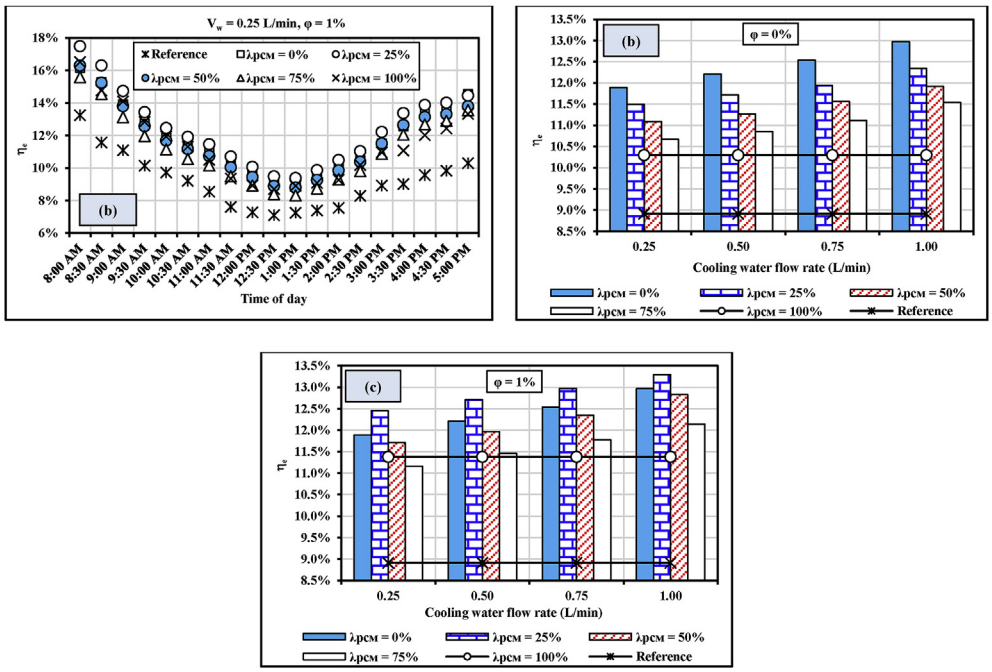

Fig. 12. PV electrical efficiency at different PCM occupation ratios; (a) Instantaneous values at $\dot{V}_w = 0.25$ L/min, $\varphi = 1\%$, (b) Average values at $\varphi = 0\%$, (c) Average values at $\varphi = 1\%$.

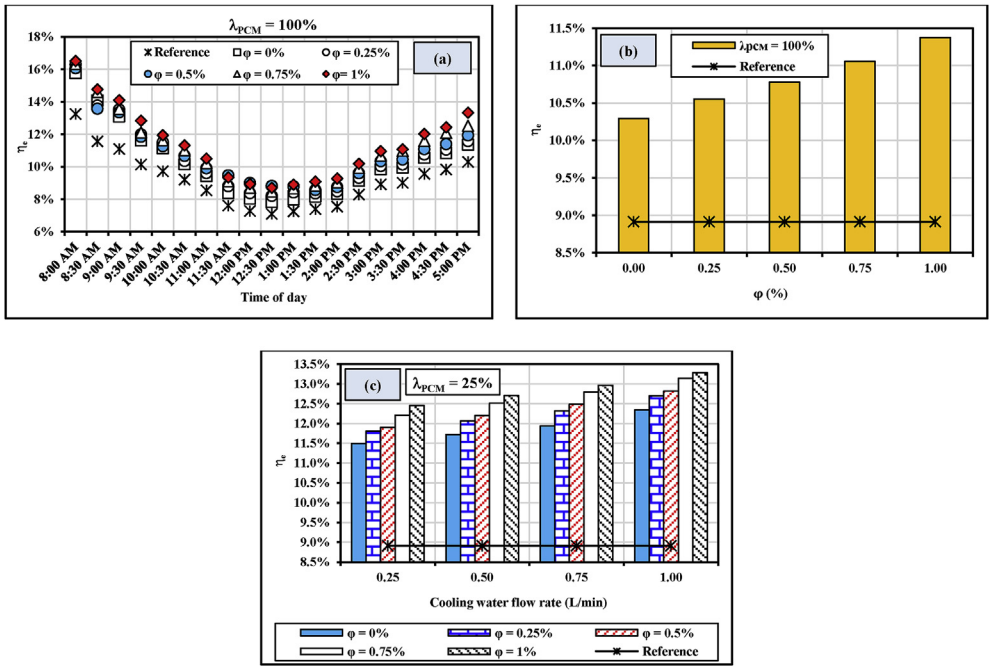

Fig. 13. PV electrical efficiency at different nanoparticles concentrations; (a) Instantaneous values, (b) Average values at $\lambda_{PCM} = 100\%$, (c) Average values at $\lambda_{PCM} = 25\%$.

the electrical output power of the water-cooled panels is not the same of the percentage increase in their electrical efficiencies as they consume a part of their output in the pumping power required to circulate the water in the system. Fig. 15 demonstrates the percentage change in the electrical output power of the cooled panels when compared with that of the reference cell at different PCM occupation ratios.

From Fig. 15a, it is presented that the 100% water-cooled panels provide the highest percentage increase in the electrical output power compared with using pure PCM/water cooling method. Additionally, from Fig. 15b–e, it is noticed that the compound cooling technique; 25% (Al_2O_3/PCM) + 75% water, provides the highest percentage increase in the electrical output power when compared with other techniques at the same conditions. This percentage decreases with increasing the PCM occupation ratio and increases with increasing the water flow rate. Compared with the reference cell, at 25% Al_2O_3/PCM (75% water), the average percentage increase in the electrical output power is augmented from 25% to 29.7%, while at 75% Al_2O_3/PCM (25% water), this percentage is augmented from 20.9% to 25% when the water flow rate increases

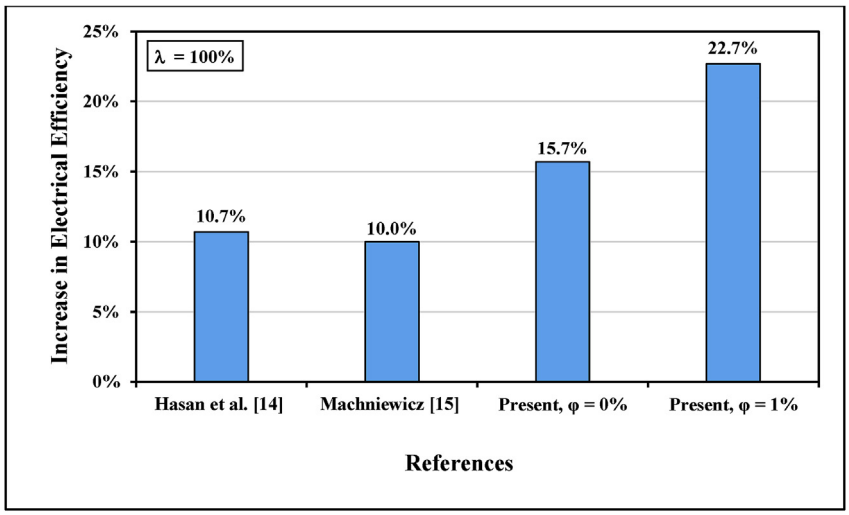

Fig. 14. Comparison of the increase in present PV electrical efficiency with other researchers ($(\lambda_{PCM} = 100\%)$.

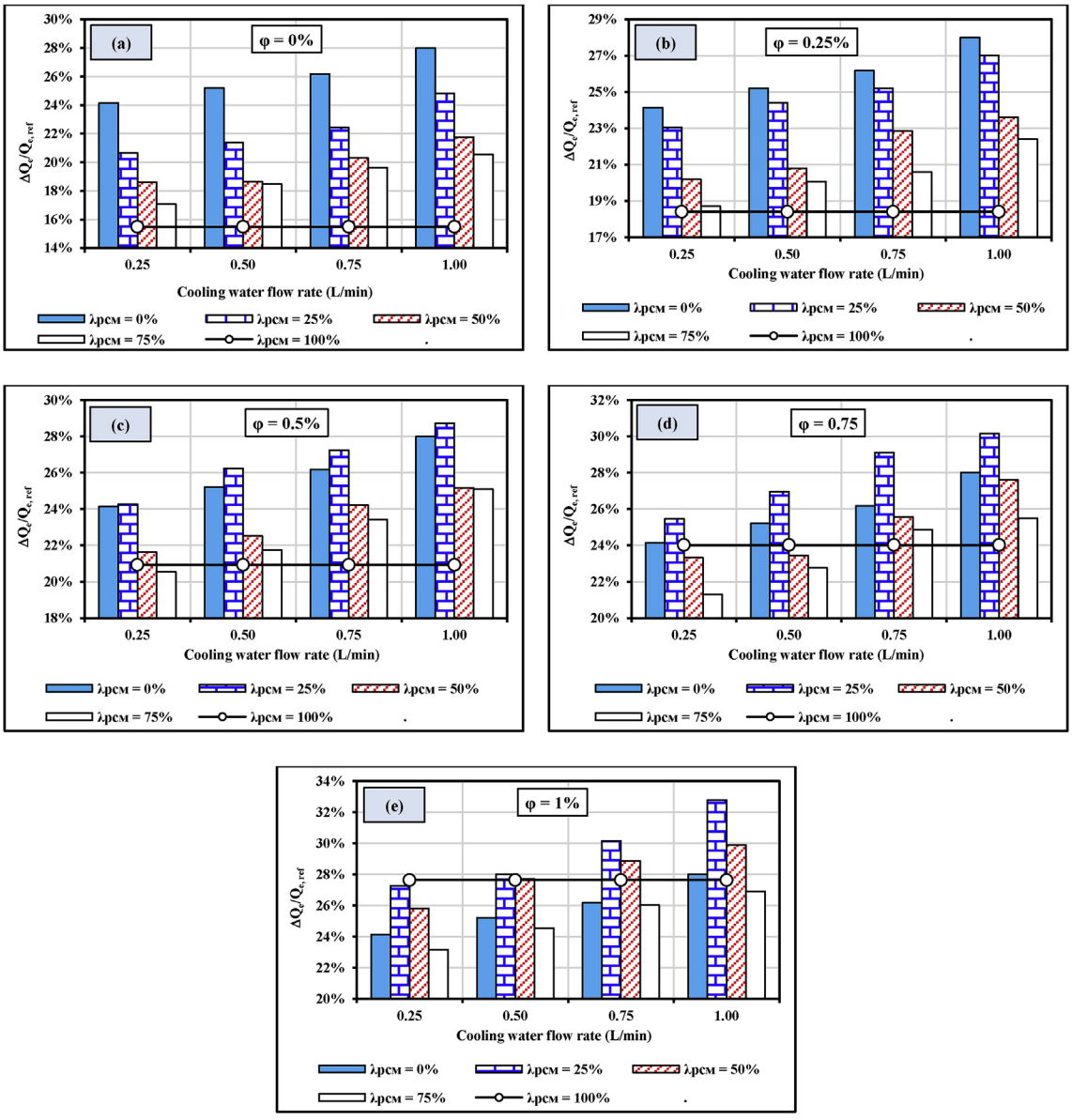

Fig. 15. Average percentage change in the electrical output power of the cooled panels at different Al_2O_3/PCM occupation ratios; (a) $\varphi = 0\%$, (b) $\varphi = 0.25\%$, (c) $\varphi = 0.5\%$, (d) $\varphi = 0.75\%$ and (e) $\varphi = 1\%$.

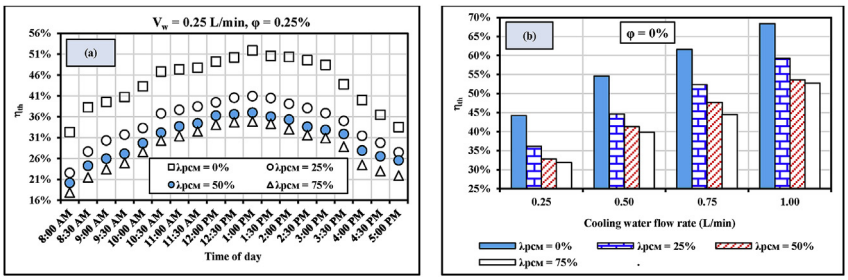

Fig. 16. PV thermal efficiency at different Al_2O_3/PCM occupation ratios; (a) Instantaneous values, (b) Average values.

from 0.25 to 1.0 L/min, respectively. While the percentage increase in the electrical output power is 21.1% for the 100% (Al_2O_3/PCM)-cooled panel.

It is evident also in Fig. 15 that the electrical output power of the 100% water-cooled panels is higher than that of the cooled panel using a PCM or Al_2O_3/PCM mixture only. Nevertheless, the usage of the water as an active enhancement technique has many constraints such as;

- The availability of the water in the places at which the panels are installed.
- The pumping power needed to flow the water through the channels.
- The maintenance that may be required for the pump.
- The lower temperature of the cooling water where it may not be available at all times of the day, and even it is available, from the domestic water supply, geothermal water, river or sea, etc., its temperature may not be constant throughout all times of the day.
- The water-cooling system is relatively complex.

Therefore, although the usage of the PCM as a cooling technique for the PV panel does not provide the highest electrical efficiency or the electrical output power, it may be a superior solution for the cell cooling as it solves these problems. The PCM does not need any additional power or costs during modules operation, and it can be used in numerous applications in which the water cannot be used.

7.3. Panel thermal efficiency

One of the benefits of using the water as a cooling medium for the PV panels is that it provides a hybrid PVT system. In this case, the solar cell is considered as a preheater for the water and saves a part of the thermal energy required in any heating process. Fig. 16 presents a sample of the obtained instantaneous and average thermal efficiencies of the cell at different Al_2O_3/PCM occupation ratios, while Fig. 17 shows a sample of the reported thermal efficiency at different Al_2O_3 nanoparticles concentrations.

It is clearly obvious in Figs. 16a and 17a that the cell thermal efficiency exhibits also the same trend as the solar radiation intensity. In addition, it is evident from Fig. 16 that the thermal efficiency decreases with increasing the PCM occupation. This is because of the increase in the heat energy transferred to the PCM from the panel, which minimizes the heat energy transferred to the water. It is shown also that the thermal efficiency increases with increasing the water flow rate. At $\lambda_{PCM} = 0\%$, the average thermal efficiency increases from 44.2% to 68.4%, while at $\lambda_{PCM} = 75\%$, it is augmented from 27.2% to 48.6% when the water flow rate increases from 0.25 to 1.0 L/min, respectively. Additionally, Fig. 17 displays that the thermal efficiency decreases with increasing the Al_2O_3 nanoparticles loading especially before 1 p.m. This may be due to increasing PCM latent heat of fusion, which allows the more heat storage in the Al_2O_3/PCM mixture. While the effect of the nanoparticles loading is a slight after 1 p.m., at which the solar intensity decreases and the PCM with higher nanoparticles concentration has more storage heat energy but at a smaller melting point.

7.4. Panel overall exergy efficiency

Figs. 18 and 19 display a sample of the reported instantaneous and average exergy efficiencies of the cells, respectively, at different Al_2O_3/PCM occupation ratios.

It is clear from Fig. 18 that the cooled panels provide a higher overall exergy efficiency than the uncooled cell. In addition, it is seen that employing $\lambda_{PCM} = 0\%$ always gives the highest overall exergy efficiency. Additionally, it is shown in Fig. 19 that the exergy efficiency increases with increasing the water flow rates. At $\lambda_{PCM} = 0\%$, the exergy efficiency increases from 12.9% to 13.6% when the water flow rate increases from 0.25 to 1.0 L/min, respectively. Compared with the reference cell ($\eta_{o,\ ex} = 8.9\%$), the average percentage increase in the exergy efficiency is 44.2% and 52.3%, respectively. Furthermore, it is seen from Figs. 18 and 19 that the exergy efficiency decreases gradually with increasing the PCM occupation ratio. Compared with the reference cell, the average percentage increase in the exergy efficiency is 45.8% and 32.6%, at $\lambda_{PCM} = 25\%$ and 75%, respectively. In addition, when all the channels

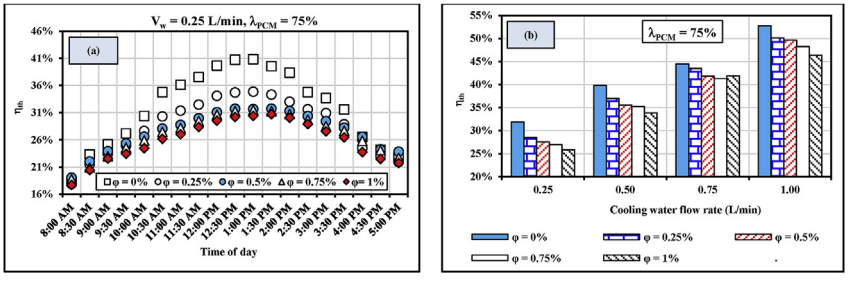

Fig. 17. PV thermal efficiency at different Al_2O_3 nanoparticles concentrations; (a) Instantaneous values, (b) Average values.

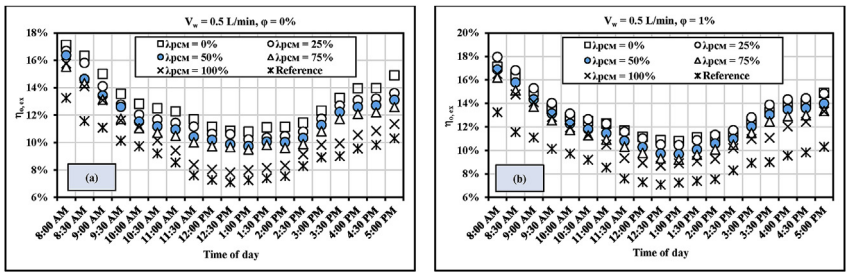

Fig. 18. Instantaneous PV exergy efficiency at different PCM occupation ratios; (a) $\varphi = 0\%$ and (b) $\varphi = 1\%$.

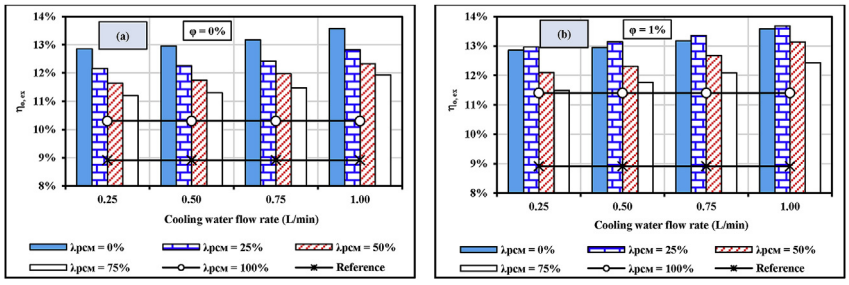

Fig. 19. Average PV exergy efficiency at different PCM occupation ratios; (a) $\varphi = 0\%$ and (b) $\varphi = 1\%$.

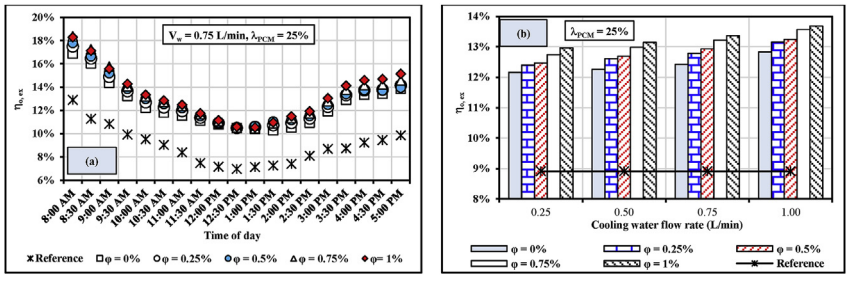

Fig. 20. PV exergy efficiency at different nanoparticles concentrations; (a) Instantaneous values, (b) Average values.

are 100% employed with Al_2O_3/PCM mixture, the average exergy efficiency is 10.9%, which corresponds to a percentage increase of 22.7% with comparison with that of the reference panel. Fig. 20 shows a sample of the recorded instantaneous and average exergy efficiencies of the modules at different Al_2O_3 nanoparticles concentrations.

From Fig. 20, it is clearly shown that the cell exergy efficiency slightly increases with increasing the nanoparticles concentration in the PCM. Compared with the reference cell, the average percentage increase in the exergy efficiency is 37.6% and 41.3% at $\varphi = 0.25\%$ and 1%, respectively.

8. Experimental correlations

Using the present data, experimental correlations are presented to predict η_e, η_{th}, and $\eta_{o,\,ex}$ of the PV module. They are correlated as a function of the cooling water mass flux (M), the PCM occupation ratio (λ_{PCM}), and the Al_2O_3 nanoparticles mass concentration (φ) as follows;

$$\eta_e = 0.123\,(1+M)^{0.043}(1+\lambda_{PCM})^{-0.279}\,(1+\varphi)^{0.096} \tag{13}$$

$$\eta_{th} = 0.435\,(1+M)^{0.584}(1+\lambda_{PCM})^{-1.526}\,(1+\varphi)^{0.14} \tag{14}$$

$$\eta_{o,\,ex} = 0.128\,(1+M)^{0.076}(1+\lambda_{PCM})^{-0.364}\,(1+\varphi)^{0.064} \tag{15}$$

Eqs. (13)–(15) are valid for $0 \le M \le 5.31\text{kg/s.m}^2$, $0 \le \lambda_{PCM} \le 100\%$, and $0 \le \varphi \le 1\%$. Comparisons of the experimental η_e, η_{th}, and $\eta_{o,\,ex}$ with those predicted by the developed correlations are demonstrated in Fig. 21.

It is obvious that the presented correlations are in good agreements with the present data; the data falls of the proposed equations within maximum deviations of ±4.3%, ±7.3% and ±4.5% for η_e, η_{th}, and $\eta_{o,\,ex}$, respectively.

9. Conclusions

This work provides an experimental investigation on the performance characteristics of a PV module cooling effect using a compound technique; water and/or Al_2O_3/PCM mixture with several nanoparticles loadings and cooling water flow rates through straight aluminium channels beneath the cell. The ranges of the investigated parameters are $0 \le M \le 5.31\text{kg/s.m}^2$, $0 \le \lambda_{PCM} \le 100\%$, and $0 \le \varphi \le 1\%$. The following conclusions can be expressed;

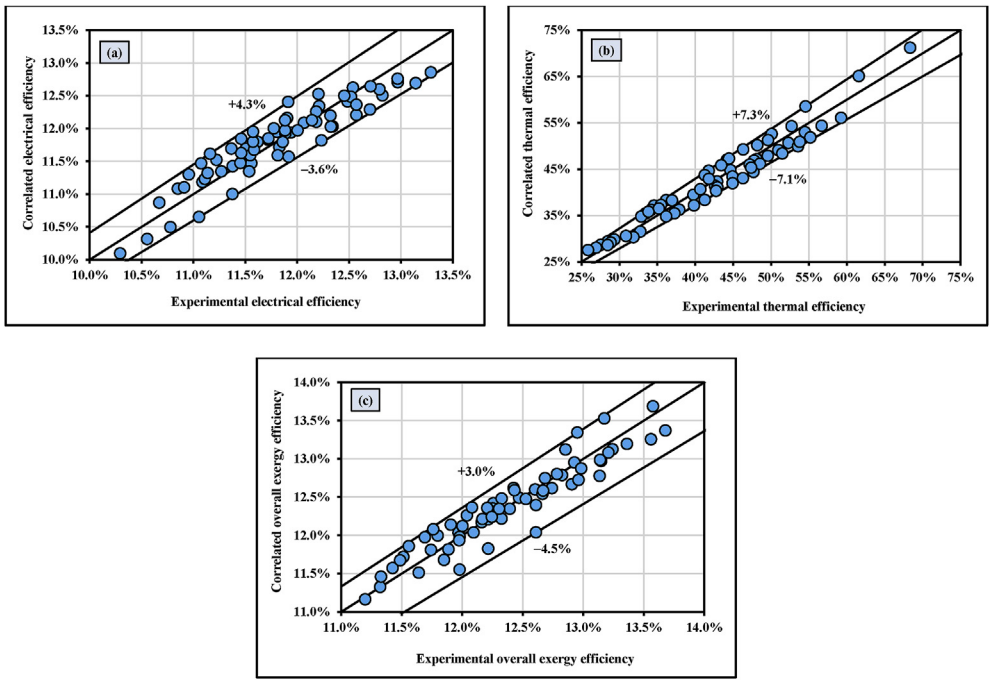

Fig. 21. Comparison of experimental values with that correlated by Eqs. (13)–(15); (a) η_e, (b) η_{th}, (c) $\eta_{o,\,ex}$.

1. The PV characteristics are directly influenced by the solar radiation intensity.
2. Applying the cooling system whether using water and/or Al_2O_3/PCM mixture provides a noticeable drop in the cells temperature.
3. Compared with employing pure PCM, employing 100% water in the channels provides the smallest module temperature and the highest η_e, η_{th}, and $\eta_{o,\,ex}$ and the highest percentage increase in the electrical output power.
4. Increasing the Al_2O_3 nanoparticles loading in the PCM and the cooling water flow rate and decreasing the Al_2O_3/PCM mixture occupation in the channels reduce the panel temperature, while they augment η_e, η_{th}, and $\eta_{o,\,ex}$.
5. The Al_2O_3 nanoparticles concentration of $\varphi = 1\%$ makes the compound technique (Al_2O_3/PCM + water) better than the cooling with 100% water at the same operating conditions.
6. Applying $\lambda_{PCM} = 25\%$ ($\varphi = 1\%$) + 75% water (1 L/min) achieves the lowest cell temperature and the highest η_e, η_{th}, and $\eta_{o,\,ex}$.
7. Although the Al_2O_3/PCM of $\lambda_{PCM} = 100\%$ does not provide the highest electrical efficiency or the electrical output power, it may be a superior solution for PV cooling as it solves the problems that face the usage of the cooling water.
8. Experimental correlations are presented to estimate the electrical, thermal and overall exergy efficiencies of the PV module.

Appendix

In the current investigation, the root-sum-square combination of the influences the individual variables as developed by Kline and McClintock [38] are utilized to calculate the uncertainty in all parameters. The maximum uncertainties are as follows;

$$\frac{\omega_{A_{PV}}}{A_{PV}} = \pm\sqrt{\left(\frac{\omega_{W_{PV}}}{W_{PV}}\right)^2 + \left(\frac{\omega_{L_{PV}}}{L_{PV}}\right)^2} = \pm\sqrt{\left(\frac{1}{550}\right)^2 + \left(\frac{1}{670}\right)^2} = \pm 0.0024 = \pm 0.24\% \tag{16}$$

$$\frac{\omega_{A_{ch}}}{A_{ch}} = \pm\sqrt{\left(\frac{\omega_{W_{ch}}}{W_{ch}}\right)^2 + \left(\frac{\omega_{L_{ch}}}{L_{ch}}\right)^2} = \pm\sqrt{\left(\frac{0.5}{25}\right)^2 + \left(\frac{0.5}{25}\right)^2} = \pm 0.0283 = \pm 2.83\% \tag{17}$$

$$\frac{\omega_{Vl_{ch}}}{Vl_{ch}} = \pm\sqrt{\left(\frac{\omega_{A_{ch}}}{A_{ch}}\right)^2 + \left(\frac{\omega_{L_{PV}}}{L_{PV}}\right)^2} \pm\sqrt{(0.0283)^2 + \left(\frac{1}{670}\right)^2} = \pm 0.0283 = \pm 2.83\% \tag{18}$$

$$\omega_{T_{PV,\,f}} = \omega_{T_{PV,\,b}} = \pm\sqrt{4(0.25\;\omega_T)^2} = \pm\sqrt{4(0.25{*}0.5)^2} = \pm 0.25^{\circ}C \tag{19}$$

$$\omega_{T_{PV,\,f}} = \omega_{T_{PV,\,b}} = \pm\sqrt{2\left(0.5\;\omega_{T_{PV,\,b}}\right)^2} = \pm\sqrt{2(0.5{*}0.25)^2} = \pm 0.18^{\circ}C \tag{20}$$

$$\omega_{\Delta T_t} = \pm\sqrt{\left(\omega_{T_{t,\,o}}\right)^2 + \left(\omega_{T_{t,\,i}}\right)^2} = \pm\sqrt{2(0.5)^2} = \pm 0.71^{\circ}C \tag{21}$$

$$\omega_{\dot{V}} = \pm\sqrt{\left(\frac{1}{1}{*}0.01\right)^2 + \left(\frac{-2}{1^2}{*}\left(\frac{1}{60}\right)\right)^2} = \pm 0.0348\;L/min = \frac{\pm 0.0348}{2}{*}100 = \pm 1.74\% \tag{22}$$

$$\frac{\omega_{\dot{m}_w}}{\dot{m}_w} = \pm\sqrt{\left(\frac{\omega_{\rho_w}}{\rho_w}\right)^2 + \left(\frac{\omega_{\dot{V}_w}}{\dot{V}_w}\right)^2} = \pm\sqrt{(0.001)^2 + (0.0174)^2} = 0.01674 = \pm 1.74\% \tag{23}$$

$$\frac{\omega_M}{M} = \pm\sqrt{\left(\frac{\omega_{\dot{m}_w}}{\dot{m}_w}\right)^2 + \left(\frac{\omega_{A_{ch}}}{A_{ch}}\right)^2} = \pm\sqrt{(0.01674)^2 + (0.0283)^2} = 0.0329 = \pm 3.29\% \tag{24}$$

$$\frac{\omega_{P_{PV}}}{P_{PV}} = \pm\sqrt{\left(\frac{\omega_I}{I}\right)^2 + \left(\frac{\omega_V}{V}\right)^2} = \pm\sqrt{(0.01)^2 + (0.01)^2} = \pm 0.0141 = \pm 1.41\% \tag{25}$$

$$\frac{\omega_{P_{in}}}{P_{in}} = \pm\sqrt{\left(\frac{\omega_{G_s}}{G_s}\right)^2 + \left(\frac{\omega_{A_{PV}}}{A_{PV}}\right)^2} = \pm\sqrt{(0.05)^2 + (0.0024)^2} = \pm 0.05 = \pm 5\% \tag{26}$$

$$\frac{\omega_{\eta_e}}{\eta_e} = \pm\sqrt{\left(\frac{\omega_{P_{PV}}}{P_{PV}}\right)^2 + \left(\frac{\omega_{P_{in}}}{P_{in}}\right)^2} = \pm\sqrt{(0.0141)^2 + (0.05)^2} = \pm 0.052 = \pm 5.2\% \tag{27}$$

$$\frac{\omega_{Q_{th}}}{Q_{th}} = \pm\sqrt{\left(\frac{\omega_{\dot{m}_w}}{\dot{m}_w}\right)^2 + \left(\frac{\omega_{Cp_w}}{Cp_w}\right)^2 + \left(\frac{\omega_{\Delta T_w}}{\Delta T_w}\right)^2} = \pm\sqrt{(0.01674)^2 + (0.01)^2 + \left(\frac{\omega_{\Delta T_w}}{\Delta T_w}\right)^2} \tag{28}$$

$$\frac{\omega_{\eta_{th}}}{\eta_{th}} = \pm\sqrt{\left(\frac{\omega_{Q_{th}}}{Q_{th}}\right)^2 + \left(\frac{\omega_{P_{in}}}{P_{in}}\right)^2} = \pm\sqrt{(0.0331)^2 + (0.05)^2} = \pm 0.0588 = \pm 5.88\% \tag{29}$$

$$\omega_{\eta_{o,ex}} = \pm\sqrt{(\omega_{\eta_e})^2 + \left(\left[1 - \frac{T_a}{T_{w,o}}\right]\omega_{\eta_{th}}\right)^2 + \left(\eta_{th}\left[1 + \frac{T_a}{T_{w,o}^2}\right]\omega_{T_{w,o}}\right)^2} = \pm 7.1\% \tag{30}$$

References

[1] C. Huang, H. Sung, K. Yen, Experimental study of photovoltaic/thermal (PV/T) hybrid system, Int. J. Smart Grid Clean Energy 2 (2) (2013) 148–151.
[2] A.N. Mahureand, V.M. Kriplani, Review of heat transfer enhancement techniques, Int. J. Eng. Res. Technol. 5 (3) (2012) 241–249.
[3] M.R. Salem, K.M. Elshazly, R.Y. Sakr, R.K. Ali, Experimental Study on Convective Heat Transfer and Pressure Drop of Water-Based Nanofluid inside Shell and Coil Heat Exchanger, Ph.D. Dissertation, Faculty of Engineering at Shoubra, Benha University, Egypt, 2014.
[4] S. Jakhar, M.S. Soni, N. Gakkhar, Historical and recent development of concentrating photovoltaic cooling technologies, Renew. Sustain. Energy Rev. 60 (2016) 41–59.
[5] A. Akbarzadeh, T. Wadowski, Heat Pipe-based cooling systems for photovoltaic cells under concentrated solar radiation, Appl. Therm. Eng. 16 (1) (1996) 81–87.
[6] W.G. Anderson, P.M. Dussinger, D.B. Sarraf, S. Tamanna, Heat pipe cooling of concentrating photovoltaic cells, in: Photovoltaic Specialists Conference. PVSC '08. 33rd IEEE, 2008.
[7] H.J. Huang, S.C. Shen, H.J. Shaw, Design and fabrication of a novel hybrid structure heat pipe for a concentrator photovoltaic, Energies 5 (12) (2012) 4340–4349.
[8] J.K. Tonui, Y. Tripanagnostopoulos, Performance improvement of PV/T solar collectors with natural air flow operation, Sol. Energy 82 (2008) 1–12.
[9] M.J. Huang, P.C. Eames, B. Norton, Thermal regulation of building-integrated photovoltaics using phase change materials, Int. J. Heat Mass Transf. 47 (2004) 2715–2733.
[10] M.J. Huang, P.C. Eames, B. Norton, Phase change materials for limiting temperature rise in building integrated photovoltaics, Sol. Energy 80 (2006) 1121–1130.
[11] M.J. Huang, P.C. Eames, B. Norton, Comparison of a small-scale 3D PCM thermal control model with a validated 2D PCM thermal control model, Sol. Energy Mater. Sol. Cells 90 (2006) 1961–1972.
[12] M.J. Huang, The effect of using two PCMs on the thermal regulation performance of BIPV systems, J. Solar Energy Mater. Solar Cells 95 (2011) 957–963.
[13] C.J. Ho, A.O. Tanuwijava, C. Lai, Thermal and electrical performance of a BIPV integrated with a microencapsulated phase change material layer, Energy Build. 50 (2012) 331–338.
[14] A. Hasan, S.J. McCormack, M.J. Huang, B. Norton, Energy and cost saving of a photovoltaic-phase change materials (PV-PCM) System through temperature regulation and performance enhancement of photovoltaics, Energies 7 (2014) 1318–1331.
[15] A. Machniewicz, D. Knera, D. Heim, Effect of transition temperature on efficiency of PV/PCM panels, Energy Procedia 78 (2015) 1684–1689.
[16] F. Hachem, B. Abdulhay, M. Ramadan, H. El Hage, M. Gad El Rab, M. Khaled, Improving the performance of photovoltaic cells using pure and combined phase change materials – experiments and transient energy balance, Renew. Energy 107 (2017) 567–575.
[17] L. Tan, A. Date, G. Fernandes, B. Singh, S. Ganguly, Efficiency gains of photovoltaic system using latent heat thermal energy storage, Energy Procedia 110 (2017) 83–88.
[18] A. Hasan, J. Sarwar, H. Alnoman, S. Abdelbaqi, Yearly energy performance of a photovoltaic-phase change material (PV-PCM) system in hot climate, Sol. Energy 146 (2017) 417–429.
[19] S.A. Nada, D.H. El-Nagar, H.M.S. Hussein, Improving the thermal regulation and efficiency enhancement of PCM Integrated PV modules using nano particles, Energy Convers. Manag. 166 (2018) 735–743.
[20] S. Khanna, K.S. Reddy, T.K. Mallick, Optimization of finned solar photovoltaic phase change material (finned PV PCM) system, Int. J. Therm. Sci. 130 (2018) 313–322.
[21] S. Khanna, K.S. Reddy, T.K. Mallick, Performance analysis of tilted photovoltaic system integrated with phase change material under varying operating conditions, Energy 133 (2018) 887–899.
[22] X. Yang, L. Sun, Y. Yuan, X. Zhao, X. Cao, Experimental investigation on performance comparison of PV/T-PCM system and PV/T system, Renew. Energy 119 (2018) 152–159.
[23] A.S. Joshi, A. Tiwari, Energy and exergy efficiencies of a hybrid photovoltaic thermal (PV/T) air collector, Renew. Energy 32 (2007) 2223–2241.
[24] M. Abdolzadeh, M. Ameri, Improving the effectiveness of a PV water pumping system by spraying water over the front of photovoltaic cells, Renew. Energy 34 (2009) 91–96.
[25] H.G. Teo, P.S. Lee, M.N.A. Hawlader, An active cooling system for photovoltaic modules, Appl. Energy 90 (2012) 309–315.
[26] M. Elmir, R. Mehdaoui, A. Mojtabi, Numerical simulation of cooling a solar cell by forced convection in the presence of a nanofluid, Energy Procedia 18 (2012) 594–603.
[27] H. Bahaidarah, Abdul Subhan, P. Gandhidasan, S. Rehman, Performance evaluation of a PV (photovoltaic) module by back surface water cooling for hot climatic conditions, Energy 59 (2013) 445–453.
[28] M. Ozgoren, M.H. Aksoy, C. Bakir, S. Dogan, Experimental performance investigation of photovoltaic/thermal (PV-T) system, EPJ Web Conf. 45 (2013) 01106, https://doi.org/10.1051/epjconf/20134501106.
[29] İ. Ceylana, A.E. Gürelb, H. Demircanc, B. Aksu, Cooling of a photovoltaic module with temperature controlled solar collector, Energy Build. 72 (2014) 96–101.
[30] N. Karami, M. Rahimi, Heat Transfer Enhancement in a PV cell using boehmite nanofluid, Energy Convers. Manag. 86 (2014) 275–285.
[31] A. Aldihani, A. Aldossary, S. Mahmoud, R.K. AL-Dadah, The effect of cooling on the performance of photovoltaic cells under dusty environmental conditions, Energy Procedia 61 (2014) 2383–2386.
[32] S. Nizetic, D. Coko, A. Yadav, F.G. Cabo, Water spray cooling technique applied on a photovoltaic panel: the performance response, Energy Convers. Manag. 108 (2016) 287–296.
[33] M.R. Salem, R.K. Ali, K.M. Elshazly, Experimental investigation of the performance of a hybrid photovoltaic/thermal solar system using aluminium cooling plate with straight and helical channels, Sol. Energy 157 (2017) 147–156.
[34] S. Preet, B. Bhushan, T. Mahajan, Experimental investigation of water based photovoltaic/thermal (PV/T) system with and without phase change material (PCM), Sol. Energy 155 (2017) 1104–1120.
[35] L. Colla, L. Fedele, S. Mancin, L. Danza, O. Manca, Nano-PCMs for enhanced energy storage and passive cooling applications, Appl. Therm. Eng. 110 (2017) 584–589.
[36] G. Ferre, A. Solé, C. Barreneche, I. Martorell, L.F. Cabeza, Review on the methodology used in thermal stability characterization of phase change materials, Renew. Sustain. Energy Rev. 50 (2015) 665–685.
[37] N. Putra, M. Amin, E.A. Kosasih, R.A. Luanto, N.A. Abdullah, Characterization of the thermal stability of RT 22 HC/graphene using a thermal cycle method based on thermoelectric methods, Appl. Therm. Eng. 124 (2017) 62–70.

[38] S.J. Kline, F.A. McClintock, Describing uncertainties in single-sample experiments, Mech. Eng. 75 (1) (1953) 3–8.

Nomenclatures

A: Area, m^2
Cp: Specific heat, J/kg.°C
G: Solar heat flux, W/m^2
H: Channel height, m
I: Electrical current, A
M: Mass flux, $kg/s.m^2$
ṁ: Mass flow rate, kg/s
m: Mass, kg
N: Number
P: Power, W
Q: Heat transfer rate, W
T: Temperature, °C or K
t: Time, s
V: Voltage drop, V
Vl: Volume, m^3
V̇: Volume flow rate, m^3/s
W: DC pumping power, W
w: Channel width, m

Greek Letters

η: Efficiency
φ: Nanoparticles mass concentration
Δ: Differential
γ: Gamma; the type of the used alumina nanoparticles
λ: The occupation ratio of the Al_2O_3/PCM in the channels
ρ: Density, kg/m^3
ω: Uncertainty

Scripts

a: Ambient
ave: Average
b: Back
bm: Base medium
c: Cooled
ch: Channel
e: Electrical
ex: Exergy
f: Front
H: Channel height
i: Inlet
In: Incident
m: Mass
max: Maximum
mp: Maximum power
np: Nanoparticles
o: Outlet
oc: Open circuit
o, ex: Overall exergy
opt: Optimum
P: Pump
PCM: Phase change material
PV: Photovoltaic
ref: Reference
S: Solar/sun
s: Surface
sc: Short circuit
th: Thermal
V: Volume
W: Channel width
w: Water

Acronyms and Abbreviations

Al_2O_3: Aluminum oxide
DC: Direct Current
PCM: Phase change material
PV: Photovoltaic
PVT: Photovoltaic/Thermal